Heterogeneous Formation of Particulate Nitrate under Ammonium-rich Regimes during the High $PM_{2.5}$ Events in Nanjing, China

Yu-Chi Lin[1,2,3], Yan-Lin Zhang[1,2,3*], Mei-Yi Fan[1,2,3], Mengying Bao[1,2,3]

[1.] Yale-NUIST Center on Atmospheric Environment, International Joint Laboratory on Climate and Environment Change, Nanjing University of Information Science and Technology, Nanjing, 210044, China.

[2.] Key Laboratory Meteorological Disaster; Ministry of Education & Collaborative Innovation Center on Forecast and Evaluation of Meteorological Disaster, Nanjing University of Information Science and Technology, Nanjing, 210044, China.

[3]. Jiangsu Provincial Key Laboratory of Agricultural Meteorology, College of Applied Meteorology, Nanjing University of Information Science & Technology, Nanjing 210044, China.

Corresponded to Yan-Lin Zhang (dryanlinzhang@outlook.com; zhangyanlin@nuist.edu.cn)

ABSTRACT

Particulate nitrate (NO_3^-) not only influences regional climates but also contributes to the acidification of terrestrial and aquatic ecosystems. In 2016 and 2017, four intensive online measurements of water-soluble ions in $PM_{2.5}$ were conducted in Nanjing City to investigate the potential formation mechanisms of particulate nitrate. During the sampling periods, NO_3^- was the most predominant species, accounting for 35 % of the total water-soluble inorganic ions, followed by SO_4^{2-} (33 %) and NH_4^+ (24 %). Significant enhancements of nitrate aerosols in terms of both absolute concentrations and relative abundances suggested that NO_3^- was a major contributing

species to high-$PM_{2.5}$ events (hourly $PM_{2.5}$ $\geqq$ 150 μg m^{-3}). High NO_3^- concentrations mainly occurred under NH_4^+-rich conditions, implying that the formation of nitrate aerosols in Nanjing involved NH_3. During the high-$PM_{2.5}$ events, the nitrogen conversion ratios (Fn) were positively correlated with the aerosol liquid water content (ALWC, $R > 0.72$, $p < 0.05$). Meanwhile, increasing NO_3^- concentrations regularly coincided with increasing ALWC and decreasing Ox (Ox = O_3 +NO_2). These results suggested that the heterogeneous reaction was probably a major mechanism of nitrate formation during the high-$PM_{2.5}$ events. Moreover, the average production rate of NO_3^- by heterogeneous processes was estimated to be 12.6 % h^{-1} (4.1 μg m^{-3} h^{-1}), which was much higher than that (2.5 % h^{-1}, 0.8 μg m^{-3} h^{-1}) of gas-phase reactions. This can also explain the abrupt increases of nitrate concentrations during the high $PM_{2.5}$ events. Utilization of ISORROPIA II model, we found that nitrate aerosol formation in Nanjing during the high-$PM_{2.5}$ events was HNO_3-limited. This indicated that control of NOx emissions will be able to efficiently reduce airborne nitrate concentrations and improve the air quality in this industrial city.

Keywords: Nitrate aerosols, nitrogen conversion ratios, NH_4^+-rich regime, Hydrolysis of N_2O_5, Nitrate production rate

1. Introduction

Due to the rapid growth of industrialization and urbanization, particulate matter (PM) pollution has become a severe problem in China in recent years (Chan and Yao, 2008; Zhang and Cao, 2015). Fine mode particles ($PM_{2.5}$, with aerodynamic diameters less than 2.5 μm) exhibit smaller sizes and contain many toxins emitted from anthropogenic emissions (Huang et al., 2018). $PM_{2.5}$ easily penetrates the upper respiratory tract and is deposited into the human body, causing serious threats to

human health. Numerous previous studies have proven that people exposed to high $PM_{2.5}$ concentrations show increased risks of respiratory illness, cardiovascular diseases and asthma (Brauer et al., 2002; Defino et al., 2005), resulting in an increase of mortality (Nel, 2005).

Secondary inorganic aerosols (SIA), including sulfate (SO_4^{2-}), nitrate (NO_3^-) and ammonium (NH_4^+), are major constituents of $PM_{2.5}$, accounting for 25 - 60 % of the $PM_{2.5}$ mass in urban cities of China (Huang et al.,2014a; Wang et al., 2018; Yang et al., 2005; Ye et al., 2017; Zhao et al., 2013; Zhou et al., 2018). Among these species, SO_4^{2-} and NO_3^- are acidic ions which tend to be neutralized by NH_4^+. Previously, many studies suggested that SO_4^{2-} dominated SIA in urban cities of China (Kong et al., 2014; Tao et al., 2016; Yang et al., 2005; Yao et al., 2002; Zhao et al., 2013). In recent years, the Chinese government reduced its anthropogenic emissions by 62 % and 17 % for SO_2 and NOx, respectively (Zheng et al., 2018). This revealed that the reduction efficiency of SO_2 emissions were much higher than those of NOx. Consequently, nitrate has become the dominant species of SIA, especially during PM haze events (Wang et al., 2018; Wen et al., 2015; Zou et al., 2018).

In the atmosphere, ammonium nitrate (NH_4NO_3) is a major form of nitrate aerosols in fine mode particles. NH_4NO_3 is a semi-volatile species which partitions from the particle phase into the gas phase under high-temperature (T) conditions. It deliquesces when the ambient relative humidity (RH) is higher than its deliquescence relative humidity (DRH, nearly 62 % RH at atmospheric standard condition). To produce NH_4NO_3, nitrogen oxides (NO_x) and ammonia (NH_3) undergo a series of chemical reactions. NO_x mostly emits as fresh NO, which is subsequently oxidized to NO_2 and reacts with hydroxyl (OH) radicals to generate nitric acid (HNO_3), and then HNO_3 reacts with NH_3 to yield NH_4NO_3 particles as listed in R1 and R2 (Calvert and Stockwell, 1983). Particulate NH_4NO_3 formation rate is profoundly dependent on the

ambient T and RH since both parameters influence the equilibrium constant of NO_3^- and NH_4^+ between the particle and gas phases, as listed in R2 (Lin and Cheng, 2007).

$$NO_{2(g)} + OH_{(g)} \rightarrow HNO_{3(g)} \qquad k_1 \qquad (R1)$$

$$HNO_{3(g)} + NH_{3(g)} \rightarrow NH_4NO_{3(s,\,aq)} \qquad k_2 \qquad (R2)$$

Here, k_1 and k_2 are the reaction rate and equilibrium constant of R1 and R2, respectively. The equilibrium constant k_2 can be expressed as the product of HNO_3 and NH_3.

Heterogeneous reactions have been considered an important mechanism of nitrate formation during nighttime. As listed in R3, liquid HNO_3 is produced by the hydrolysis of dinitrogen pentoxide (N_2O_5) on aerosol surfaces (Brown & Stutz, 2012; Chang et al., 2011; Mental et al., 1999; Wahner et al., 1998). Liquid HNO_3 can be neutralized by NH_4^+, which is produced from the conversion of gaseous NH_3. Nitrate aerosols yielded from both R2 and R3 require NH_3, and therefore these processes of NO_3^- formation occur under NH_4 -rich conditions. Sometimes, there is not enough NH_3 (NH_4^+) to react (to be neutralized) with HNO_3 (NO_3^-) after complete neutralization by H_2SO_4. Under this condition, HNO_3 tends to react (or to be neutralized) with other alkaline species such as Ca-rich dust ($CaCO_3$), and subsequently, nitrate aerosol is produced under a NH_4^+-poor regime (Goodman et al., 2000).

$$N_2O_{5(g)} + H_2O_{(l)} \rightarrow 2HNO_{3(aq)} \qquad (R3)$$

The Yangtze River Delta (YRD) region is one of the well-known polluted areas in China (Zhang and Cao, 2015). Different from the case of dramatic elevated sulfate aerosol levels in Beijing (Wang et al., 2016), nitrate aerosols seemed to be a major contributing species during haze days in the YRD region (Wang et al., 2015; Wang et al., 2018). The formation mechanisms of nitrate in Nanjing have not yet been well

understood, especially during high PM events. In this study, four intensive online measurements of water-soluble ions in $PM_{2.5}$ were conducted in Nanjing City in 2016 and 2017. The data provided information on the hourly evolution of water-soluble inorganic ions (WSIIs) in the industrial city. The NO_3^- distributions under different NH_4^+ regimes (NH_4^+-poor and NH_4^+-rich conditions) were also discussed. Finally, we investigated the potential formation mechanisms of nitrate aerosols and their production rates during high-$PM_{2.5}$ events based on the online measurements.

2. Methodology

2.1 Sampling site

Particulate WSIIs and inorganic gases were continuously monitored at Nanjing University of Information Science and Technology (NUIST) located in the northern part of Nanjing City (see Figure S1). In addition to vehicle emissions, petroleum chemical refineries and steel manufacturing plants situated in the northeast and east direction at a distance of approximately 5 km are also major anthropogenic emissions near the receptor site. Four intensive campaigns were conducted from March 2016 to August 2017. During each experiment, the hourly concentrations of WSIIs in $PM_{2.5}$ and inorganic gases were continuously observed. Meanwhile, the hourly $PM_{2.5}$ mass, NO_2 and O_3 concentrations along with the ambient T and RH were acquired from the Pukou air quality monitoring station which is located to the southwest of the receptor site.

2.2 Instruments

To monitor the hourly concentrations of WSIIs (Cl^-, NO_3^-, SO_4^{2-}, Na^+, NH_4^+, K^+, Mg^{2+} and Ca^{2+}), an online Monitor for Aerosols and Gases (MAGAR, Applikon-ENC, The Netherlands) instrument with a $PM_{2.5}$ inlet was employed. Using this instrument,

the WSIIs in $PM_{2.5}$ were collected by a stream jet aerosol collector, while acidic (HCl, HONO, HNO_3 and SO_2) and basic gases (NH_3) were dissolved in a hydrogen peroxide solution on a wet rotation denuder (ten Brink et al., 2007; Griffith, et al., 2015). The liquid samples were then collected with syringe pumps and analyzed by ion chromatography (IC). Before each campaign, a seven-point calibration curve of each species was made, and an internal standard solution (LiBr) was used to check instrumental drifts. The method detection limits (MDLs) of Cl^-, NO_3^-, SO_4^{2-}, Na^+, NH_4^+, K^+, Mg^{2+} and Ca^{2+} were, 0.01, 0.04, 0.06, 0.05, 0.05, 0.07, 0.05 and 0.11 μg m^{-3}, respectively. For gases, the MDLs were 0.07, 0.09, 0.06, 0.02 and 0.08 μg m^{-3} for HCl, HONO, HNO_3, SO_2 and NH_3, respectively.

2.3 ISORROPIA-II model

In this work**,** we used the ISORROPIA-II model to calculate the aerosol liquid water content (ALWC). ISORROPIA II is a thermodynamic equilibrium model which is built based on the Na^+ - Cl^- - Ca^{2+} - K^+ - Mg^{2+} - SO_4^{2-} - NH_4^+ - NO_3^- - H_2O aerosol system (Fountoukis & Nenes, 2007). This model has been successfully used to estimate the liquid water content in aerosols with uncertainty of ~ 20 % compared to the observed ALWC (Bian et al., 2014; Guo et al., 2015; Liu et al., 2017). This underestimation might be due to the missed species in ISORROPIA II, organic aerosols, which contributed approximately 27 % to total ALWC (Bougiatioti et al., 2007). Here, the model was computed as a “forward problem”, in which the quantities of aerosol- and gas-phase compositions along with the T and RH were well known. Additionally, the modeled values were determined using the “metastable” mode, which indicated that the aerosol compositions were assumed to be composed of an aqueous solution (Liu et al., 2017). The details of this model can be found elsewhere (Fountoukis and Nenes, 2007). In this work, the observed concentrations of total

nitrate (HNO_3+NO_3^-), total ammonium (NH_3 + NH_4^+), total chloride (HCl + Cl-), SO_4^{2-}, Na^+, K^+, Mg^{2+} and Ca^{2+} along with measured ambient T and RH served as input of ISORROPIA II model.

2.4 Potential source contribution function

Potential source contribution function (PSCF) is a method to identify the potential source regions of air pollutants. It has also been widely used to differentiate local emission from long-range transported pollution (Zhang et al., 2013; Hui et al., 2018) based on the trajectory analysis calculated from GDAS (Global Data Assimilation System), which processed by the National Centers for Environmental Prediction (NCEP). The zone of concern is divided into $i \times j$ small equal grid cells and then PSCF in the *i-jth* cell ($PSCF_{ij}$) can be defined as (Polissar et al., 1999):

$$PSCF_{ij} = \frac{m_{ij}}{n_{ij}} \quad (1)$$

where m_{ij} is the number of "high nitrate pollution" trajectory endpoints in the *i-jth* cell and n_{ij} is the total number of trajectory endpoints fallen into the *i-jth* cell. In this study, the 80th percentile value of nitrate concentration was treated as "high nitrate pollution" threshold. To reduce the uncertainty caused by the small values of n_{ij}, the weighting function of W_{ij} has to be considered (Polissar et al., 1999):

$$W_{ij} = \begin{cases} 1.00; & 80 < n_{ij} \\ 0.70; & 20 < n_{ij} \leqq 80 \\ 0.42; & 10 < n_{ij} \leqq 20 \\ 0.05; & n_{ij} \leqq 10 \end{cases}$$

In this study, the domain of the study area was in a range of 20-55 °N and 105-135 °E;

the resolution of grid cell was 0.5°×0.5°.

3. Results and discussion

3.1 Overview of water-soluble inorganic ions

Four intensive online measurements of WSIIs in $PM_{2.5}$ were carried out in Nanjing City from March 2016 to August 2017. Figure 1a plots the time series of the hourly $PM_{2.5}$ mass concentrations during the sampling periods. As seen, the hourly $PM_{2.5}$ mass concentrations varied from 5 to 252 μg m^{-3} with a mean value of 58 ± 35 μg m^{-3}. Compared with the 24-hour guideline (25 μg m^{-3}) suggested by the World Health Organization (WHO), our average $PM_{2.5}$ concentration (58 μg m^{-3}) was 2.3 times higher. This indicated that PM pollution in Nanjing City was a serious problem. During the campaigns, several high-$PM_{2.5}$ events with hourly $PM_{2.5}$ concentrations of higher than 150 μg m^{-3} were observed in the springtime and wintertime. These high $PM_{2.5}$ levels lasted for more than 3 hours, with obviously elevated NO_3^-. The details of nitrate formation during the high-$PM_{2.5}$ hours will be discussed in the following sections.

Figure 1b shows time series of the hourly concentrations of SIA species, including SO_4^{2-}, NO_3^- and NH_4^+. The lack of data from March 7 to 14, 2016 was due to a malfunction of the MARGA instrument. During the sampling periods, the NO_3^- concentrations varied from 0.1 to 85.1 μg m^{-3} with a mean value of 16.7 ± 12.8 μg m^{-3}. The SO_4^{2-} concentrations ranged from 1.7 to 96.2 μg m^{-3} and averaged 14.9 ± 9.1 μg m^{-3}. The NH_4^+ concentrations fluctuated between 0.8 and 44.9 μg m^{-3} with a mean value of 10.7 ± 6.7 μg m^{-3}. On average, SIA accounted for 91 % of the total water-soluble inorganic ions (TWSIIs) during the entirety of the sampling periods (see Figure 2a). Among these species, NO_3^- accounted for 35 % of the TWSIIs, followed by SO_4^{2-} (33 %) and NH_4^+ (24 %). The abundances of other ions, including Cl^-, K^+,

Ca^{2+}, Na^{+} and Mg^{2+}, were 5, 2, 1, 0.7 and 0.3 %, respectively. Figure S2 shows the scatter plot of the equivalent concentrations of the cations (Na^{+}, NH_4^{+}, K^{+}, Mg^{2+} and Ca^{2+}) and anions (Cl^{-}, SO_4^{2-} and NH_4^{+}). As seen, good correlations (R = 0.98 -0.99, with a significance level $p<0.05$) between cations and anions were found during the various sampling periods. The ratio of cation-to-anion was very close to 1.0 during each season, reflecting an ionic balance. This also indicated that our data exhibited good quality and was able to be used for the further analysis of scientific issues.

All SIA species exhibited similar seasonal patterns, with lower concentrations in the summer, especially for NO_3^{-}. The average concentrations of nitrate were 6.7 and 5.7 μg m^{-3} in the summertime of 2016 and 2017, respectively (see Figure S3). These values were much lower than those observed during other seasons. The local meteorological conditions, which were favorable for the dilution of air pollution, were one of the reasons for the declined NO_3^{-} concentrations during the hot seasons (Zhang and Cao, 2015). Another important reason for this effect was attributed to the formation process of $PM_{2.5}$ nitrate, which is very sensitive to the ambient T and RH (Lin and Cheng, 2007). Figure S4a depicts the theoretical equilibrium constants of partitioned NO_3^{-} and NH_4^{+} between the particle and gas phase ($HNO_{3(g)} + NH_{3(g)} \rightarrow NH_4NO_{3(s,\ aq)}$ as seen in R2) under different T and RH conditions. The details of calculation approach of the theoretical equilibrium constants are described in *Supplementary S1*. Note that the *Y-axis* is presented on a log scale. The theoretical equilibrium constants increased exponentially with increasing ambient temperature but decreased with increasing RH. This indicated that NH_4NO_3 would be partitioned into the gas phase due to high equilibrium constants under high-temperature and low-RH conditions. Figure S4b illustrates the time series of the theoretical and observed equilibrium constants during the sampling periods. As can be seen, most of the observed equilibrium constants were higher than the theoretical ones, suggesting that

233 NH_4NO_3 aerosols were produced in Nanjing during the sampling periods. Obviously,
234 higher theoretical and lower observed equilibrium constants were found during the
235 summer. This suggested that more NO_3^- and NH_4^+ would tend to be partitioned into
236 the gas phase, resulting in lower particulate nitrate concentrations during hot seasons
237 (Lin and Cheng, 2007).

238 Apart from seasonal variations, pronounced diurnal patterns were also found for
239 SIA species (see Figure 3). NO_3^- exhibited similar diel cycles during different seasons,
240 with higher concentrations in the early morning (3 a.m. - 7 a.m.) and lower levels
241 between 2 p.m. and 5 p.m. The high nitrate concentrations in the early morning might
242 be caused by the nitrate formation via heterogeneous reaction in the dark, and gas-
243 phase oxidation after sunrise and the subsequent condensation on pre-existing
244 particles before the temperature increased and RH decreased afterwards. Moreover,
245 the lower planet boundary layer (PBL) might be another reason for enhanced nitrate
246 in the early morning. However, the lower concentrations of nitrate during the daytime
247 might be attributed to the higher PBL, and high temperatures, which inhibited the
248 build-up of nitrate, especially during the summertime. In terms of sulfate, higher
249 concentrations were observed between 6 am. and 1 p.m., indicating that the formation
250 rate of sulfate was higher than the removal/dilution rate, leading to an increase of the
251 sulfate concentration during the daytime. The diurnal patterns of NH_4^+ mimicked
252 those of NO_3^-, showing lower concentrations during the daytime. This was explained
253 by the drastic decrease of particulate NH_4NO_3 concentrations under high temperatures
254 and low relative humidity, resulting in lower NH_4^+ levels during the daytime.
255

256 **3.2 Enhancements of nitrate at high $PM_{2.5}$ levels**

257 Figure S5 shows the scatter plots of NO_3^-, SO_4^{2-} and NH_4^+ against $PM_{2.5}$. As
258 seen, the slopes of NO_3^- (NO_3^- vs. $PM_{2.5}$ mass), SO_4^{2-} and NH_4^+ were 0.30, 0.24 and

0.19, respectively. This suggested that the increasing rate of NO_3^- during the high-$PM_{2.5}$ events was higher than those of other SIA species. At high $PM_{2.5}$ levels ($PM_{2.5} \geq 150$ μg/m^3), NO_3^-, SO_4^{2-} and NH_4^+ contributed 39, 28 and 24 % of the TWSIIs, respectively (Figure 2b). However, the relative abundances of NO_3^-, SO_4^{2-} and NH_4^+ during low $PM_{2.5}$ concentrations (hourly $PM_{2.5} < 35$ μg/m^3, see Figure 2c) were 29, 37 and 23 %, respectively. In recent years, dramatically enhanced amounts of nitrate aerosols during high-PM events have been observed at many urban sites in China (Wen et al., 2015; Wang et al., 2017; 2018; Zou et al., 2018). For instance, Zou et al. (2018) found that the nitrate concentrations during the occurrence of polluted air in Beijing and Tianjin were almost 14 times higher than those on relatively clean days ($PM_{2.5} < 75$ μg/m^3), and the enhancement ratio of nitrate was much higher than that (5.3) of sulfate. Wang et al. (2018) noted that the enhancement ratio of NO_3^- (~6) between haze and clear days in Ningbo of the YRD region was much higher than that of SO_4^{2-} (~3). These findings suggested that NO_3^- was a major contributing species to fine particles during haze days since its increasing ratio between haze and non-haze days was much higher than those of other SIA species, such as sulfate and ammonium.

3.3 PSCF result of high nitrate pollution

During the high $PM_{2.5}$ pollution, significant enhanced nitrate aerosols in terms of both absolute concentration and relative abundance to TWSIIs were found. Next, we tried to use PSCF analysis to identify whether local emission or long-range transported pollution was the major source of high nitrate concentrations at the receptor site. In this work, the 80th percentile values of nitrate concentration was selected as "high nitrate pollution" threshold for PSCF analysis. Figure 4 plots the PSCF result of high nitrate pollution in Nanjing during the sampling periods. The

region corresponding to high PSCF value grid is a potential source region of nitrate aerosols. As can be seen, the areas with high PSCF value (>0.8) were regularly local areas surrounding by Nanjing while PSCF values from other long-distance areas were lower than 0.2. This suggested that NO_3^- aerosols in Nanjing during the high nitrate pollution were likely from local emissions rather than long-range transported sources.

3.4 Nitrate formation under different ammonium regimes

Ammonium is a major species that neutralizes particulate SO_4^{2-} and NO_3^-. In the atmosphere, SO_4^{2-} competes with NO_3^- for NH_4^+ during their formation processes, and therefore, the relationship between the molar ratios of NO_3^-/SO_4^{2-} and NH_4^+/SO_4^{2-} can give us a hint for understanding the formation of NO_3^- under different ammonium regimes (Pathak et al., 2009; He et al., 2012; Tao et al., 2016). In an ammonium-rich regime, the HNO_3 produced by both gas oxidation and heterogeneous process reacts (or neutralizes) with "excess-ammonium" (excess-NH_4^+) at a NH_4^+/SO_4^{2-} molar ratio > 2 (theoretical value in an NH_4^+-rich regime) when sulfate is completely neutralized by NH_4^+ to form $(NH_4)_2SO_4$ (Squizzato et al., 2013; Ye et al., 2011). In contrast, nitrate can be found under ammonium-poor conditions with a theoretical NH_4^+/SO_4^{2-} value that should be less than 2 (Pathak et al., 2009). Under NH_4^+-poor conditions, HNO_3 reacts with other cations, such as the calcium carbonate, frequently found in natural dust.

Figure 5 shows the scatter plot of the molar ratios of NO_3^-/SO_4^{2-} against NH_4^+/SO_4^{2-}. It is found that good correlations existed between NO_3^-/SO_4^{2-} and NH_4^+/SO_4^{2-} under NH_4^+-rich regimes, with a coefficient of determination (R^2) of 0.84 - 0.94 in the different seasons (see in Table 1). Utilizing the linear regression model, we suggested that nitrate aerosols (in NH_4^+-rich regimes) began to form when the NH_4^+/SO_4^{2-} molar ratios exceeded the criterion values of 1.7-2.0 during the different

311 seasons (Table 1). The criterion value can be calculated as absolute value of
312 "intercept" dividing by slope in each linear regression model (He et al., 2012). The
313 criterion values below 2 suggested that part of the sulfate might have existed in other
314 forms, such as ammonium bisulfate. On the other hand, under ammonium-rich
315 conditions, nitrate concentrations should be positively proportional to "excess-NH_4^+"
316 concentrations, a relationship which was defined as [excess-NH_4^+] = (NH_4^+/SO_4^{2-} -
317 criterion value) × [SO_4^{2-}] (Pathak et al., 2009) (sulfate is in the units of nmol m^{-3}
318 here). The criterion values were acquired from the regression models, as listed in
319 Table 1. The results revealed that the excess-NH_4^+ concentrations varied from -283 to
320 1422 nmol m^{-3} (see Figure 6), and only 1 % of data showed deficit-NH_4^+ conditions,
321 reflecting that NO_3^- formation in Nanjing occurred primarily under the NH_4^+-rich
322 conditions. Moreover, the excess-NH_4^+ had apparent diurnal cycles, with higher
323 concentrations in the early morning and lower concentrations at midday and in the
324 early afternoon (see Figure 3, where we converted the units from nmol m^{-3} to μg m^{-3}).
325 The diurnal patterns of NO_3^- mimicked those of the excess-NH_4^+. This also suggested
326 that particulate NO_3^- formation occurred mainly under NH_4^+-rich conditions. Figure 6
327 illustrates the relationship between the nitrate and excess-NH_4^+ molar concentrations
328 during the sampling periods. The nitrate molar concentrations correlated linearly with
329 the excess-NH_4^+ molar concentrations with a slope of approximately 1.0, which was
330 consistent with the molar ratio of reaction between HNO_3 and NH_3. Interestingly,
331 some scattered points were found in high ammonium concentrations (excess-NH_4^+ ≧
332 900 nmol m^{-3} ~ 16.2 μg m^{-3}), implying that residual NH_4^+ might be presented in
333 another form such as NH_4Cl under high-NH_4^+ conditions. On the contrary, NO_3^-
334 aerosols can be produced without involving NH_3; therefore, NO_3^- did not correlate
335 well with the excess NH_4^+ under a NH_4^+-poor regime.
336 In this study, high nitrate concentrations were always found under NH_4^+-rich

regimes, elucidating that nitrate production during high PM levels in Nanjing had to be involved with NH_3 or NH_4^+. Figure 6 also shows the nitrate concentrations against the excess-NH_4^+ observed in various cities of China during the summertime (Pathak et al., 2009; Griffith et al., 2015). In Beijing and Shanghai, high nitrate concentrations during the summertime were found under NH_4^+-deficient conditions, which was very different from the findings of this work. In these studies (Pathak et al., 2009; Griffith et al., 2015), the high nitrate concentrations associated with NH_4^+-poor conditions might be due to the lower excess-NH_4^+ concentrations under high-SO_4^{2-} conditions at that time since the strict control of SO_2 emissions by the Chinese government started in 2010 (Zheng et al., 2018). In recent years, the reduction of anthropogenic SO_2 emissions decreased the airborne SO_4^{2-} concentrations, resulting in more excess-NH_4^+ and leading to nitrate aerosol formation under NH_4^+-rich regimes. This argument can be supported by the recent results shown in Figure S6, in which high nitrate concentrations in Beijing were always found under NH_4^+-rich regimes.

3.5 Nitrate formation mechanism during high-$PM_{2.5}$ episodes

In this section, we attempted to explore the formation mechanisms of nitrate aerosols during high $PM_{2.5}$ levels. Here, nitrogen conversion ratio (Fn) was used to evaluate the conversion capability of NO_2 to total nitrate (TN, TN=HNO_3 + NO_3^-), and it can be defined as (Khoder, 2002; Lin et al., 2006):

$$F_n = \frac{GNO_3^- + PNO_3^-}{GNO_3^- + PNO_3 + NO_2} \quad (1)$$

where GNO_3^- and PNO_3^- represent the NO_2 concentrations in nitric acid and particulate nitrate, respectively, with the units of μg m^{-3}. The results showed that the Fn values during the sampling periods varied from 0.01 to 0.57 with a mean value of 0.14 ± 0.09 (see Figure 1e). This value was comparable to that (0.17) in Taichung,

363 Taiwan, where both gas-oxidation and heterogeneous reaction were the dominant
364 formation mechanisms of atmospheric HNO_3 (or NO_3^-) (Lin et al., 2006). However,
365 our Fn value was 2.3 time higher than that (0.06) in Dokki, Egypt (Khoder, 2002).
366 The reason of significant discrepancy of Fn between this work and that in Dokki was
367 not clearly understood, but it might be attributed to different formation processes of
368 HNO_3. In Dokki, gas-phase oxidation was the dominant pathway of HNO_3 production
369 while heterogeneous process (R3) played an important role in HNO_3 formation in
370 addition to gas-phase oxidation in Nanjing, especially during the high-$PM_{2.5}$ events
371 (discussed later). The reaction rate of HNO_3 by heterogeneous process was much
372 higher than that by gas-phase oxidation (Calvert and Stockwell, 1983) and therefore,
373 the Fn value was much higher in this study. On the other hand, Fn displayed
374 significant diurnal cycles, with the highest value in the early morning (see in Figure
375 3). This elevated Fn coincided with increasing ALWC, suggesting heterogeneous
376 reaction since ALWC is one of the key parameters which favors the transformation of
377 N_2O_5 to liquid HNO_3 in this process (also indicated that nitrate formation was
378 associated with heterogeneous process). On the contrary, a second peak of Fn was
379 found in the early afternoon when Ox ($Ox = NO_2 + O_3$, an index of the oxidation
380 capacity) concentrations increased, but ALWC decreased. This suggested that the
381 HNO_3 formation might be mainly associated with the gas-phase reaction of NO_2 +
382 OH during the daytime; also reflected that nitrate formation was via gas-phase
383 oxidation.
384 Assuming that long-range transported nitrate can be neglected in this study (in
385 section 3.3), we attempted to analyze the correlations of Fn vs. OH and Fn vs. ALWC
386 to investigate whether gas-phase oxidation or heterogeneous reactions might be the
387 dominant mechanism of nitrate production. In this work, the OH radical
388 concentrations were not measured; hence, we used O_X as a proxy of OH. The ALWC

was acquired by computing the ISOPROPIA II model as described in section 2.3. Figure 7 illustrates the scatter plots of Fn against Ox and ALWC in both daytime and nighttime aerosol samples during the high-$PM_{2.5}$ events. Fn correlated well with the ALWC, with a correlation coefficient (R) of 0.72 and 0.76 ($p < 0.05$) at daytime and nighttime samples, respectively. However, a poor correlation was found between Fn and Ox (R was 0.17 and 0.52 for the daytime and nighttime samples, $p>0.05$). This implied that nitrate formation during the high-$PM_{2.5}$ events in Nanjing was likely attributed to heterogeneous reactions. This result was consistent with recent conclusions reached by oxygen isotope techniques, in which the hydrolysis of N_2O_5 in preexisting aerosols was found to be a major mechanism of NO_3^- formation (Chang et al., 2018).

3.6 Case study and production rate of NO_3^- during $PM_{2.5}$ episodes

Figure 8 shows several high-$PM_{2.5}$ events observed from March 3 to 6 in 2016. In case I, the high $PM_{2.5}$ concentrations started at 6 p.m. on March 3 and ended at 3 a.m. on March 4. During this event, the SO_4^{2-} and NH_4^+ concentrations remained at almost constant levels, but the NO_3^- concentrations revealed a slight enhancement. In the early morning of March 4, the NO_3^- concentrations increased from 39.4 to 47.8 μg m^{-3} within 4 hours, resulting in a nitrate production rate of 2.3 μg m^{-3} h^{-1} (~5.5 % h^{-1}, the calculation of NO_3^- production rate can be seen in the *Supplementary S2*). In case II, high $PM_{2.5}$ concentrations were observed from 8. a.m. to 2. p.m. on March 4. The NO_3^- concentrations were much higher than those of SO_4^{2-}, indicating nitrate-dominated aerosols. In this case, the NO_3^- concentrations increased from 38.1 to 51.2 μg m^{-3} within 6 hours, suggesting that the increasing rate of NO_3^- was 1.0 μg m^{-3} h^{-1} (2.4 % h^{-1}). Since the high NO_3^- concentrations occurred under high-Ox and low-ALWC conditions, this suggested that the gas-phase reaction of NO_2 + OH might be

415 the dominant source of NO_3^- production in this event. In case III, a rapid growth of the
416 $PM_{2.5}$ mass was found around midnight, along with a dramatic increase of NO_3^-
417 concentrations from 11 p.m. on March 4 (31.0 μg m^{-3}) and maximizing at 1 a.m. the
418 next day (64.5 μg m^{-3}). The increasing rate of NO_3^- was estimated to be 11.4 μg m^{-3} h^{-1}
419 (~26.7 % h^{-1}), which was much higher than those in case I and II. The high-nitrate
420 event was found under increasing ALWC and decreasing Ox concentration conditions,
421 suggesting that nitrate production occurred through heterogeneous processes. In case
422 IV, the enhancements of all SIA species coincided with increasing ALWC and
423 declining Ox concentrations. Again, the enhancement of nitrate was likely attributed
424 to heterogeneous reactions rather than to gas-phase processes. In these events, the
425 NO_3^- production rate was estimated to be 5.0 μg m^{-3} h^{-1} (~ 15.4 % h^{-1}).
426 Through the sampling periods, a total of twelve high $PM_{2.5}$ events were found, and the
427 NO_3^- concentrations increased significantly during all the episodes (see in Table S1).
428 Seven episodes suggested that heterogeneous processes ($N_2O_5 + H_2O$) might be a
429 major pathway for nitrate formation since elevated NO_3^- levels coincided with
430 increasing AWLC and decreasing Ox (or Ox remaining at a constant level). Among
431 these heterogeneous process events, five cases (Case III, Case IX, Case X, Case XI
432 and Case XII in Table S1) were observed during the nighttime (5 p.m. – 6 a.m. on the
433 next day). This suggested that approximately 70 % heterogeneous reaction of nitrate
434 production was observed in the dark. In these events, the average NO_3^- growth rate
435 was 12.6 ± 7.3 % h^{-1} (4.1 ± 3.6 μg m^{-3} h^{-1}). This value was in agreement with those in
436 the literatures which the production rate of nitrate via heterogeneous reaction were
437 14.3 % h^{-1} by both field measurements and laboratory works (Calvert and Stockwell,
438 1983; Pathak et al., 2011). On the contrary, NO_3^- concentrations rose with increasing
439 Ox and decreasing ALWC in two $PM_{2.5}$ episodes, indicating gas-phase processes
440 (NO_2 + OH). As listed in Table S1, these gas-phase reaction cases occurred mainly

during the daytime. The average production rate of NO_3^- in the gas-oxidation reaction cases averaged 2.5 ± 0.1 % h^{-1} (0.8 ± 0.3 μg m^{-3} h^{-1}), which was in line with that (2.4 % h^{-1}) in the subtropical polluted urban site that nitrate aerosols were mainly from gas-oxidation process (Lin et al., 2007). Moreover, we also found some cases in which the elevated NO_3^- might have been from both gas-phase and heterogeneous reactions, and the corresponding NO_3^- growth rate was approximately 7.5 ± 3.0 % h^{-1}(2.5 ± 0.2 μg m^{-3} h^{-1}). In conclusion, enhancements of NO_3^- in Nanjing usually occurred under increased ALWC and decreased Ox conditions, indicating that heterogeneous reactions provided the dominant pathway of nitrate formation during the $PM_{2.5}$ episodes. Moreover, the average growth rate of NO_3^- (12.6 % h^{-1}) by heterogeneous processes was 5 times higher than that (2.5 % h^{-1}) of gas-phase reactions. This might explain the abrupt increase of nitrate concentrations during the high $PM_{2.5}$ events.

3.7 HNO_3/NH_3 limitation of nitrate aerosol formation

In Nanjing, high nitrate concentrations occurred mainly under NH_4^+-rich regimes, indicating the involvement of atmospheric NH_3. This also demonstrated that both HNO_3 and NH_3 were crucial precursors for particulate nitrate formation. In this section, we attempted to discuss whether HNO_3 or NH_3 was the limited factor for nitrate formation in Nanjing during the high-$PM_{2.5}$ events. ISORROIPA II model is capable of predicting concentrations of particulate ions in addition to ALWC under thermodynamic equilibrium between gas- and aerosol-phase of these ions (Tang et al., 2016). In section 3.5, we used this model to estimate ALWC. Indeed, the output data also included concentrations of ionic species. Figure S7 illustrates the scatter plots of modeled results against observations of NO_3^-, SO_4^{2-} and NH_4^+ in Nanjing during the sampling periods. Good correlations were found between modeled results and

observations (R^2=0.97-0.99 with all slopes of approximately 1.0), suggesting that ISORROPIA II had a good performance in prediction of SIA species. As a result, we can use ISORROPIA II model to test sensitivity of HNO_3 and NH_3 to particulate nitrate concentrations (Guo et al., 2018).

Figure 7 shows the contour plot of the simulated nitrate concentrations depending on the various total nitrate (TN) and total ammonium (TA, TA=NH_3 + NH_4^+) levels under thermodynamic equilibrium conditions computed by ISORROPIA II model. The details of considered chemical reactions in ISORROPIA II model can be seen elsewhere (Fountoukis & Nenes, 2007). Here, sulfate concentrations were assumed to be 10 and 60 μg m^{-3} for the tests of different sulfate conditions. The average concentrations of total chloride (HCl + Cl^-, 1.3 μg m^{-3}), Na^+ (0.2 μg m^{-3}), K^+ (0.8 μg m^{-3}), Mg^{2+} (0.1 μg m^{-3}) and Ca^{2+} (0.5 μg m^{-3}) along with ambient T (20 °C) and RH (62 %) at the receptor site during the sampling period served as input data in this model. The results showed that the lower simulated NO_3^- concentrations was found in the higher SO_4^{2-} case under the same TN and TA levels. This was attributed to less NH_4NO_3 formation under higher SO_4^{2-} conditions since SO_4^{2-} would compete with NO_3^- for NH_4^+.

According to the simulated results, we can roughly split the plots into two parts: one is HNO_3-limited area (right), and another is NH_3-limited region (left). The observed TN and TA concentrations (pink circles) in Nanjing are also plotted in this figure. Most of the observed data sets were mainly affected by TN under a low-SO_4^{2-} case. Under a high-SO_4^{2-} condition, the observed data fell into TA-limited under a low-TN and -TA regime, but fell into TN-limited in high-TA and-TN regimes. During the sampling period, high nitrate concentrations always occurred under the high TN and TA conditions, highlighting that nitrate aerosol production in Nanjing during the high $PM_{2.5}$ levels was mainly control by HNO_3. Therefore, control of NOx emissions,

493 which reduced HNO_3 concentrations, might be an important way to decrease airborne
494 nitrate concentrations and ameliorate the air quality in Nanjing.
495
496 **4. Conclusion and remarks**
497 Four intensive online measurements of water-soluble ions in $PM_{2.5}$ were carried
498 out in Nanjing City in 2016 and 2017 to realize the evolutions of SIA and the potential
499 formation mechanisms of particulate nitrate. During the sampling periods, the average
500 concentrations of NO_3^-, SO_4^{2-} and NH_4^+ were 16.7, 14.9 and 10.7 μg m^{-3}, respectively.
501 This indicated that NO_3^- dominated the SIA. Significant seasonal variations and
502 diurnal cycles were found for all SIA species. The low NO_3^- concentrations observed
503 during the summer daytime could be attributed to the enhanced theoretical and
504 declined observed equilibrium constants of NO_3^- and NH_4^+ between gas- and particle-
505 phase. Obvious enhancements of NO_3^- were found in terms of both absolute
506 concentrations and relative abundances during the $PM_{2.5}$ episodes, indicating that
507 NO_3^- was a major contributing species to $PM_{2.5}$. Different from the results obtained in
508 Beijing and Shanghai, high nitrate concentrations always occurred under NH_4^+-rich
509 regimes. The nitrogen conversion ratio, Fn, correlated well with the ALWC but not
510 with Ox during high-$PM_{2.5}$ episodes. These findings indicated that NO_3^- aerosols at
511 the receptor site were mainly produced by heterogeneous reactions ($N_2O_5 + H_2O$) with
512 the involvement of NH_3. The average production rate of NO_3^- from heterogeneous
513 reactions was estimated to be 12.6 % h^{-1}, which was 5 time higher than that of gas-
514 phase reactions. According to the observations and ISORROPIA II simulated results,
515 particulate nitrate formation in Nanjing was HNO_3-limited, suggesting that the control
516 of NOx emissions will be able to decrease the nitrate concentration and improve the
517 air quality in this industrial city.
518 During the last decade, the mass ratios of nitrate-to-sulfate in $PM_{2.5}$ in the YRD

519 region have been found to range from 0.3 to 0.7 (Lai et al., 2007; Wang et al., 2003;
520 2006; Yang et al., 2005; Yao et al., 2002), reflecting that the SO_4^{2-} concentration was
521 much higher than the NO_3^- concentration. In the current study, the average mass ratio
522 of nitrate-to-sulfate was 1.1. Indeed, high nitrate-to-sulfate mass ratios of > 1 were
523 also observed in other mega-cities of China recently (Ge et al., 2017; Wei et al., 2018;
524 Ye et al., 2017; Zou et al., 2018). The elevated nitrate-to-sulfate ratio should be due to
525 the dramatic reduction of SO_2 emissions. The enhanced ratio also suggests that we
526 should pay more attention to develop some strategies for the reduction of NOx
527 emissions, leading to declined nitrate concentrations in the atmosphere and
528 improvement of the air quality in China.
529
530 **Data availability**
531 All the data used in this paper are available from the corresponding author upon
532 request (dryanlinzhang@outlook.com or zhangyanlin@nuist.edu.cn).
533
534 **Author contributions**
535 YLZ conceived and designed the study. YCL analyzed the data and wrote the
536 manuscript with YLZ. FM and MB performed aerosol sampling and data analyses
537 with YCL.
538
539 **Competing interests**
540 The authors declare that they have no conflict of interest.
541
542 **Acknowledgements**
543 This study was financially supported by the National Key R&D Program of China
544 (Grant No. 2017YFC0212700), the Natural Scientific Foundation of China (Nos.

41761144056, 91644103 and 41977185) and Jiangsu Innovation & Entrepreneurship Team.

References

Baasandorj, M., Hoch, S. W., Bares, R., Lin, J. C., Brown, S. S., Millet, D. B., Martin, R., Kelly, K., Zarzana, K. J., Whiteman, C. D., Bube, W. P., Tonnesen, G., Jaramillo, J. C. and Sohl, J.: Coupling between chemical and meteorological processes under persistent coal-air poor conditions: evolution of wintertime $PM_{2.5}$ events and N_2O_5 observation in Utah's Salt Lake Valley. *Environ. Sci. Technol.*, **51**, 5941-5950, https://doi.org/10.1021/acs.est.6b06603, 2017.

Bian, Y. X., Zhao, C. S., Ma, N., Chen, J., and Xu, W. Y.: A study of aerosol liquid water content based on hygroscopicity measurements at high relative humidity in the Northern China Plain. *Atmos. Chem. Phys.,* **14**, 6417-6426, https://doi.org/10.5194/acp-14-6417-2014, 2014.

Bougiatioti, A., Nikolaou, P., Stavroulas, I., Kouvarakis, G., Weber, A., Nenes, R., Kanakidou, M., and Mihalopoulos, N.: Particle water and pH in the eastern Mediterranean: source variability and implication of nutrient availability. *Atmos. Chem. Phys.,* **16**, 4579-4591, https://doi.org/10.5194/acp-7-4639-2007, 2007.

Brauer, M., Hoek, G., Vliet, V. P., Meliefste, K., Fischer, P. H., Wijga, A., Koopman, L. P., Neijens, H. J., Gerritsen, J., Kerkhof, M., Heinrich, J., Bellander, T., and Brunekreef, B.: Air pollution from traffic and the development of respiratory infections and asthmatic and allergic symptoms in children. *Am. J. Respir. Crit. Care Med.*, **166**, 1092-1098, https://doi.org/10.1146/rccm.200108-007OC, 2002.

Brown, S. S., and Stutz, J.: Nighttime radical observation and chemistry. *Chem. Soc. Rev.*, **41**, 6405-6447, https://doi.org/10.1039/c2cs35181a, 2012.

Calvert, J. G., and Stockwell, W. R.: Acid generation in the troposphere by gas-phase

chemistry. *Environ. Sci. Technol.*, **17**, 428-443, https://doi.org/10.1021/es00115a727, 1983.

Chan, C. K., and Yao, X.: Air pollution in mega cities in China. *Atmos. Enviro.,* **42**, 1-42, https://doi.org/10.1016/j.atmosenv.2007.09.003, 2008.

Chang, W. L., Bhave, P. V., Brown, S. S., Riemer, N., Stutz, J., and Dabdub, D.: Heterogeneous atmospheric chemistry, ambient measurements, and model calculations of N_2O_5: a review. *Aerosol Sc. Technol.,* **45**, 655 - 685, https://doi.org/10.1080/02786826.2010.551672, 2011.

Defino, R. J., Siotuas, C., and Malik, S.: Potential role of ultrafine particles in associations between airborne particle mass and cardiovascular health. *Environ. Health Perspect.*, **113**, 934-938, https://doi.org/10.1289/ehp.7938, 2005.

Fountoukis, C., and Nenes, A.: ISORROPIA II: a computationally efficient thermodynamic equilibrium model for K^+-Ca^{2+}-Mg^{2+}-NH_4^+-Na^+-SO_4^{2-}-NO_3^--Cl^--H_2O. *Atmos. Chem. Phys.*, **7**, 4639-4659, https://doi.org/10.5194/acp-7-4639-2007, 2007.

Ge, X., Li, L., Chen, Y., Chen, H., Wu, D., Wang, J., Xie, X., Ge, S., Ye, Z., Xu, J., and Chen, M.: Aerosol characteristics and sources in Yangzhou, China resolved by offline aerosol mass spectrometry and other techniques. *Environ. Pollut.*, **225**, 74-85, https://doi.org/10.1016/j.encpol.2017.03.044, 2017.

Goodman, A. L., Underwood, G. M., and Grassian, V. H.: A laboratory study of the heterogeneous reaction of nitric acid on calcium carbonate particles. *J. Geophys. Res. Atmos.,* **105**, 29053-29064, https://doi.org/10.1029/2000JD900396, 2000.

Griffith, S. M., Huang, X. H. H., Louie, P. K. K., and Yu, J. Z.: Characterizing the thermodynamic and chemical composition factors controlling $PM_{2.5}$ nitrate: Insights from two years of online measurements in Hong Kong. *Atmos. Environ.*, **122**, 864-875, https://doi.org/10.1016/ j.atmosenv.2015.02.009, 2015.

Guo, H., Xu, L., Bougiatioti, A., Cerully, K. M. , Capps, S. L., Heti Jr., J. R., Carton, A. G., Lee, S.-H., Bergin, M. H., Ng, N. L., Nenes, A., and Weber, R. J.: Fine particle water and pH in the southeastern United States. *Atmos. Chem. Phys.*, **15**, 5221-5228. https://doi.org/10.5194/acp-15-5211-2015, 2015.

Guo, H., Otjes, R., Schlag, P., Kiendler-Schar, A., Nenes, A., and Weber, R. J.: Effectiveness of ammonia reduction of control of fine particulate nitrate. *Atmos. Chem. Phys.*, **18**, 12241-12256. https://doi.org/10.5194/acp-18-12241, 2018, 2018.

He, K., Zhao, Q., Ma, Y., Duan, F., Yang, F., Shi, Z., and Chen, G.: Spatial and seasonal variability of $PM_{2.5}$ acidity at two Chinese megacities: insights into the formation of secondary inorganic aerosols. *Atmos. Chem. Phys.*, **12**, 1377-1395. https://doi.org/10.5194/acp-12-1377-2012, 2012.

Huang, R.-J., Zhang, Y., Bozzetti, C., Ho, K.-F., Cao, J.-J., Han, Y., Daellenbach, R., Slowik, J. G., Platt, S. M., Canonaco, F., Zotter, P., Wolf, R., Pieber, S. M., Bruns, E. A., Crippa, M., Ciarelli, G., Piazzalunga, A., Schwikkowski, M., Abbaszade, G., Schnelle-Kreis, J., Zimmerman, R., An, Z., Szidat, S., Baltensperger, U., Haddad, I. E., and Prévôt, A. H.: High secondary aerosol contribution to particulate pollution during haze events in China. *Nature*, **514**, 218-222, https://doi.org/10.1038/nature13774, 2014a.

Huang, R. J., Chen, R., Jing, M., Yang, L., Li, Y., Chen, Q., Chen, Y., Yan, J., Lin, C., Wu, Y., Zhang, R., Haddad, J. E., Prevot, A. S. H., O'Dowd, C. D., and Cao, J.: Source-specific health risk analysis on particulate trace elements: coal combustion and traffic emission as major contributors in wintertime Beijing. *Environ. Sci. Technol. 52,* 10967-10974, https://doi.org/10.1021/acs.est.8b02091.

Huang, Y., Shen, H., Chen, H., Wang, R., Zhang, Y., Su, S., Chen, Y., Lin, N., Zhong, Q., Wang, X., Liu, J., Li, B., Liu, W., and Tao, S.: Quantification of global primary

emissions of $PM_{2.5}$, PM_{10} and TSP from combustion and industrial process sources. *Environ. Sci. Technol.,* **48**, 13834-13843, https://doi.org/10.1021/es503696k, 2014b.

Hui, L., Liu, X., Tan, Q., Feng, M., An. J., Qu, Y., Zhang, Y., and Jiang, M.: Characteristics, source apportionment and contribution of VOCs to ozone formation in Wuhan, Central China. *Atmos. Environ.,* **192**, 55-71, https://doi.org/10.1016/j.atmosenv.2018.08.0642, 2018.

Khoder, M. I.: Atmospheric conversion of sulfur dioxide to particulate sulfate and nitrogen dioxide to particulate nitrate and gaseous nitric acid in an urban area. *Chemosphere*, **49**, 675-684, https://doi.org/10.1016/S0045-6535(02)00391-0, 2002.

Kong, L., Yang, Y., Zhang, S., Zhao, X., Du, H., Fu, H., Zhang, S., Cheng, T., Yang, X., Chen, J., Wu, D., Sheng, J., Hong, S., and Jiao, L.: Observation of linear dependence between sulfate and nitrate in atmospheric particles. *J. Geophys. Res. Atmos.,* **119**, 341-361, https://doi.org/10.1002/2013JD020222, 2014.

Lin, Y.-C., and Cheng, M.-T.: Evaluation of formation rates of NO_2 to gaseous and particulate nitrate in the urban atmosphere. *Atmos. Environ.,* **41**, 1903-1910, https://doi.org/10.1016/j.atmosenv.2006.10.065, 2007.

Lin, Y.-C., Cheng, M.-T., Ting, W.-Y., and Yeh, C.-R.: Characteristics of gaseous HNO_2, HNO_3, NH_3 and particulate ammonium nitrate in an urban city of central Taiwan. *Atmos. Environ.,* **40**(25), 4725-4733, https://doi.org/10.1016/j.atmosenv.2006.04.037, 2006.

Liu, M., Song, Y., Zhou, T., Xu, Z., Yan, C., Zheng, M., Wu, Z., Hu, M., Wu, Y., and Zhu, T.: Fine particle pH during severe haze episodes in northern China. *Geophys. Res. Lett.,* **44**, 5213-5222, https://doi.org/10.1002/2017GL073210, 2017.

649 Mental, T. F., Sohn, M., and Wahner, A.: Nitrate effect in the heterogeneous
650 hydrolysis of dinitrogen pentoxide on aqueous aerosols. *Phys. Chem. Chem.*
651 *Phys.*, **1**, 5451-5457, https://doi.org/10.1039/a905338g, 1999.
652 Nel, A.: Air pollution-related illness: effects of particles. *Science*, **308**, 804-806,
653 https://doi.org/10.1126/science.1108752, 2005.
654 Pan, Y., Tian, S., Zhao, Y., Zhang, L., Zhu, X., Gao, J., Huang, W., Zhou, Y., Song, Y.,
655 Zhang, Q., and Wang, Y.: Identifying ammonia hotspots in China using a national
656 observation work. *Environ. Sci. and Technol.*, **52**, 3926-3934.
657 https://doi.org/10.1021.acs/est.7b05235, 2018.
658 Pathak, R. K., Wu, W. S., and Wang, T.: Summertime $PM_{2.5}$ ionic species in four
659 major cities of China: nitrate formation in an ammonia-deficient atmosphere.
660 *Atmos. Chem. and Phys.*, **9**, 1711-1722, https://doi.org/10.5194/acp-9-1711-2009,
661 2009.
662 Pathak, R. K., Wang, T., and Wu, W. H.: Nighttime enhancement of $PM_{2.5}$ in
663 ammonia-poor atmospheric conditions in Beijing and Shanghai: Plausible
664 contributions of heterogeneous hydrolysis of N_2O_5 and HNO_3 partitioning.
665 *Atmos. Environ.,* **45**, 1183-1191, https://doi.org/10.1016/j.atmosenv.2010.09.003,
666 2011.
667 Polissar, A. V., Hopke, P. K., Paatero, P., Kaufmann, Y. J., Hall, D. K., Bodhaine, B.
668 A., Dutton, E. G., and Harris, J. M.: The aerosol at Barrow, Alaska: long-term
669 trends and source locations. Atmos. Environ., **33**, 2441-2458,
670 https://doi.org/10.1016/j.atmosenv.2018.08.0642, 2018.
671 Prabhakar, G., Parworth, C. L., Zhang, X., Kim, H., Young, D. E., Beyersdorf, A. J.,
672 Ziemba, L. D., Nowak, J. B., Bertram, T. H., Faloona, I. C., Zhang, Q., and
673 Cappa, C. D.: Observational assessment of the role of nocturnal residual-layer
674 chemistry in determining daytime surface particulate nitrate concentrations.

675 *Atmos. Chem. Phys.*, **17**, 14747-14770, https://doi.org/10.5194/acp-17-14747-
676 2017, 2017.
677 Squizzato, S., Masiol, M., Brunelli, A., Pistollato, S., Tarabotti, Z., Rampazzo, G., and
678 Pavoni, B.: Factors determining the formation of secondary inorganic aerosol: a
679 case study in the Po Valley (Italy). *Atmos. Chem. and Phys.,* **13**, 1927-1339,
680 https://doi.org/10.5194/acp-13-1927-2013, 2013.
681 Tang, X., Zhang, X., Ci, Z., Guo, J., and Wang, J.: Speciation of the major inorganic
682 salts in atmospheric aerosols of Beijing: China: measurements and comparison
683 with model. *Atmos. Environ.,* **133**, 123-134, https://doi.org/10.1016/j.atmosenv.
684 2016.03.013.
685 Tao, Y., Ye, X., Ma, Z., Xie, Y., Wang, R., Chen, J., Yang, X., and Jiang, S.: Insights
686 into different nitrate formation mechanisms from seasonal variations of secondary
687 inorganic aerosols in Shanghai. *Atmos. Environ.,* **145**, 1-9,
688 https://doi.org/10.1016/j.atmosenv.2016.09.012, 2016.
689 ten Brink, H., Otjes, R., Jongejan, P., and Slanina, S.: An instrument for semi-
690 continuous monitoring of the size-distribution of nitrate, ammonium, sulfate and
691 chloride in aerosols. *Atmos. Environ.,* **41**, 2768-2779,
692 https://doi.org/10.1016/j.atmosenv.2006.11.041, 2007.
693 Wahner, A., Mental, T. F., Sohn, M., and Stier, J.: Heterogenous reaction of N_2O_5 on
694 sodium nitrate aerosol. *J. Geophys. Res. Atmos.*, **103**, 31103-31112,
695 https://doi.org/10.1029/1998JD100022, 1998.
696 Wang, G., Wang, H., Yu, Y., Gao, S., Feng, J., Gao, S., & Wang, L.: Chemical
697 characterization of water-soluble components of PM_{10} and $PM_{2.5}$ atmospheric
698 aerosols in five locations of Nanjing, China. *Atmos. Environ.*, **37**., 2893-2902.
699 https://doi.org/10.1016/j.atmosenv.S1352-2310(03)00271-1, 2003.
700 Wang, G., Zhang, R., Geomez, M. E., Yang, L., Zamora, M. L., Hu, M., Lin, Y., Peng,

J., Guo, S., Meng, J., Li, J., Cheng, C., Hu, T., Ren, Y., Wang, Y., Gao, J., An, Z., Zhou, W., Li, G., Wang, J., Tian, P., Marrero-Ortiz, W., Secrest, J., Du, Z., Zheng, J., Shang, D., Zheng, L., Shao, M., Wang, W., Huang, Y., Wang, Y., Zhu, Y., Li, Y., Hu, J., Pan, B., Cai, L., Cheng, Y., Ji, Y., Zhang, F., Rosenfeld, D., Liss, P. S., Duce, R. A., Kolb, C. E., and Molina, M. J.: Persistent sulfate formation from London fog to Chinese haze. *Proc. Natl. Acad. Sci.*, **113**, 13630-13635, https://doi.org/ 10.1073/pnas.1616540113, 2016.

Wang, H., Lu, K., Chen, X., Zhu, Q., Chen, Q., Guo, S., Jiang, M., Li, X., Shang, D., Tang, Z., Wu, Y., Wu, Z., Zou, Q., Zheng, Y., Zheng, L., Zhu, T., Hu, M., and Zhang, Y.: High N_2O_5 concentrations observed in urban Beijing: implications of a large nitrate formation. *Environ. Sci. Technol. Lett.*, **4**, 416-420, https://doi.org/10.1021/acsestlett.7b00341, 2017.

Wang, H., Zhu, B., Shen, L., Xu, H., An, J., Xue, G., and Cao, J.: Water soluble ions in atmospheric aerosols measured in five sites in the Yantze River Delta, China: size-fractionated seasonal variation and sources. *Atmos. Environ.*, **123**(B), 370-379, https://doi.org/10.1016/j.atmosenv.2015.05.070, 2015.

Wang, W., Yu, J., Cui. Y., He, J., Xue, P., Cao, W., Ying, H., Gao, W., YIng, Y., Gao, W., Yan, Y., Hu, B., Xin, J., Wang, L., Liu, Z., Sun, Y., Ji, D., and Wang, Y.: Characteristics of fine particulate matter and its sources in an industrialized coastal city, Ningbo, Yantze River Delta, China. *Atmos. Res.*, **203**, 105-117, https://doi.org/10.1016/j.atmosres.2017.11.033, 2018.

Wang, Y., Zhuang, G., Zhang, X., Xu, C., Tang, A., Chen, J., and An, Z.: The ion chemistry, seasonal cycle, and sources of $PM_{2.5}$ and TSP aerosol in Shanghai. *Atmos. Environ.,* **40**(16), 2935-2952, https://doi.org/10.1016/j.atmosenv.2005.12.051, 2006.

Wei, L., Yue, S., Zhao, W., Yang, W., Zhang, Y., Ren, L., Han, X., Guo, Q., Sun, Y.,

727 Wang, Z., and Fu, P.: Stable sulfur isotope ratios and chemical compositions of
728 fine aerosols ($PM_{2.5}$) in Beijing, China. *Sci. Total Environ.*, **633**, 1156-1164,
729 https://doi.org/10.1016/j.scitotenv.2018.03.153, 2018.
730 Wen, L., Chen, J., Yang, L., Wang, X., Xu, C., Sui, X., Yao, L., Zhu, Y., Zhang, J.,
731 Zhu, T., and Wang, W.: Enhanced formation of particulate nitrate at a rural site on
732 the North China Plain in summer: the importance roles of ammonia and ozone.
733 *Atmos. Environ.,* **101**, 294-302, https://doi.org/10.1016/j.atmosenv.2014.11.037,
734 2015.
735 Yang, H., Yu, J. Z., Ho, S. S. H., Xu, J., Wu, W.-S., Wan, C. H., Wang, X., Wang, X.,
736 and Wang, L.: The chemical composition of inorganic and carbonaceous
737 materials in $PM_{2.5}$ in Nanjing, China. *Atmos. Environ. ,* **39**, 3735-3749,
738 https://doi.org/10.1016/j.atmosenv.2005.03.010, 2005.
739 Yao, X., Chan, C. K., Fang, M., Cadle, S., Chan, T., Mulawa, P., He, K., and Ye, B.:
740 The water-soluble ionic composition $PM_{2.5}$ in Shanghai and Beijing, China.
741 *Atmos. Environ.,* **36**, 4223-4234, https://doi.org/10.1016/j.atmosenv.2005.12.051,
742 2002.
743 Ye, X. N., Ma, Z., Zhang, J. C., Du, H. H., Chen, J. M., Chen, H., Yang, X., Gao, W.,
744 and Geng, F. H.: Important role of ammonia on haze formation in Shanghai.
745 *Environ. Res. Lett.*, **6**, 024019, https://doi.org/10.1088/1748-9326/6/2024019,
746 2011.
747 Ye, Z., Liu, J., Gu, A., Feng, F., Liu, Y., Bi, C., Xu, J., Li, L., Chen, H., Chen, Y., Dai,
748 L., Zhou, Q., and Ge, X.: Chemical characterization of fine particulate matter in
749 Changzhou, China and source apportionment with offline aerosol mass
750 spectrometry. *Atmos. Chem. .Phys.,* **17**, 2573-2592, https://doi.org/10.5194/acp-
751 17-2573-2017, 2017.
752 Zhang, R., Jing, J., Tao, J., Hsu, S.-C., Wang, G., Cao, J., Lee, C.S.L., Zhu, L., Chen,

753 Z., Zhao, Y., and Shen, Z., Chemical characterization and source apportionment
754 of $PM_{2.5}$ in Beijing: seasonal perspective. *Atmos. Chem. .Phys.,* **13**, 7053-7074,
755 https://doi.org/10.5194/acp-13-7053-20173, 2013.
756 Zhang, Y.-L., and Cao, F.: Fine particulate matters ($PM_{2.5}$) in China at a city level. *Sci.*
757 *Rep.,* **5**, 14884, https://doi.org/10.1038/srep14884, 2015.
758 Zhao, P. S., Dong, F., He, D., Zhao, X. J., Zhang, X. L., Zhang, W. Z., Yao, Q., and
759 Liu, H. Y.: Characteristics of concentrations and chemical compositions for
760 PM2.5 in the region of Beijing, Tianjin, and Hebei, China. *Atmos. Chem. Phys.,*
761 **13**, 4631-4644, https://doi.org/10.5194/acp-13-4631-2013, 2013.
762 Zheng, B., Tong, D., Li, M., Liu, F., Hong, C., Geng, G., Li, H., Li, X., Peng, L., Qi,
763 J., Yan, L., Zhang, Y., Zhao, H., Zheng, Y., He, K., and Zhang, Q.: Trends in
764 China's anthropogenic emissions since 2010 as the consequence of clean air
765 actions. *Atmos. Chem. .Phys.,* **18**(19), 14095-14111, https://doi.org/10.5194/acp-
766 18-14095-2018, 2018.
767 Zou, J., Liu, Z., Hu, B., Huang, X., Wen, T., Ji, D., Liu, J., Yang, Y., Yao, and Wang,
768 Y.: Aerosol chemical compositions in the Northern China Plain and the impact on
769 visibility in Beijing and Tianjin., *Atmos. Res.*, **201**, 235-246,
770 https://doi.org/10.1016/j.atmosres.2017.09.014, 2018.
771

772 **Table Captions**

773 Table 1 The regression models between NO_3^-/SO_4^{2-} (Y) and NH_4^+/SO_4^{2-} (X) along
774 with the criterion values of NH_4^+/SO_4^{2-} in ammonium-rich regime during the
775 sampling periods.

776

777 **Figure Captions**

778 Figure 1 Time series of concentrations in (a) $PM_{2.5}$ mass, (b) SIA species, (c) ALWC
779 and (d) Ox along with (e) Fn observed in Nanjing during the sampling
780 periods. The grey shadows represent the high $PM_{2.5}$ periods discussed in the
781 section 3.6.

782 Figure 2 Abundance of each species in TWSIIs during the (a) entire, (b) haze ($PM_{2.5} \geq$
783 150 μg m^{-3}) and (c) clear ($PM_{2.5} < 35$ μg m^{-3}) events. The numbers in the
784 parentheses are standard deviations.

785 Figure 3 Abundance of each species in TWSIIs during the (a) entire, (b) haze ($PM_{2.5} \geq$
786 150 μg m^{-3}) and (c) clear ($PM_{2.5} < 35$ μg m^{-3}) events. The numbers in the
787 parentheses are standard deviations.

788 Figure 4 The PSCF maps of high nitrate pollution.

789 Figure 5 Scatter plots of molar ratios of NO_3^-/SO_4^{2-} against NH_4^+/SO_4^{2-} in Nanjing
790 during the different seasons.

791 Figure 6 Scatter plot of NO_3^- vs. excess-NH_4^+ molar concentrations in Nanjing during
792 the different seasons. The results in Beijing, Shanghai, Guangzhou, Lanzhou
793 and Hong Kong are also shown in this figure.

794 Figure 7 Scatter plots of (a) Fn against Ox and (b) Fn against ALWC in daytime and
795 nighttime aerosol samples during the high hourly $PM_{2.5}$ concentration
796 conditions (hourly $PM_{2.5} \geqq 150$ μg m^{-3}).

797 Figure 8 Time series of concentrations in (a) $PM_{2.5}$ mass and CO, (b) SIA species

798 (NO_3^-, SO_4^{2-} and NH_4^+), (c) ALWC, Ox and NO_2 and (d) RH and T in
799 Nanjing City from March 3 to 6, 2016. The grey shadows denote $PM_{2.5}$
800 episodes. The red numbers represent NO_3^- production rate during the $PM_{2.5}$
801 episodes.
802 Figure 9 Nitrate concentrations simulated by ISORROPIA II model dependening on
803 TN and TA concentrations under (a) SO_4^{2-} = 10 μg m^{-3} and (b) SO_4^{2-} = 60
804 μg m^{-3}. The purple dots denote the observed TN and TA concentrations at
805 the receptor site during the sampling periods.
806

Table 1 The regression models between NO_3^-/SO_4^{2-} (Y) and NH_4^+/SO_4^{2-} (X) along with the criterion values of NH_4^+/SO_4^{2-} in ammonium-rich regime during the sampling periods.

Sampling periods	Regression models	Criterion values of NH_4^+/SO_4^{2-}
2016 spring	$Y = 0.71\ X - 1.27;\ R^2 = 0.87$	1.8
2016 summer	$Y = 0.67\ X - 1.22;\ R^2 = 0.86$	1.8
2017 winter	$Y = 0.81\ X - 1.50;\ R^2 = 0.91$	1.9
2017 spring	$Y = 0.95\ X - 1.91;\ R^2 = 0.94$	2.0
2017 summer	$Y = 0.79\ X - 1.32;\ R^2 = 0.84$	1.7

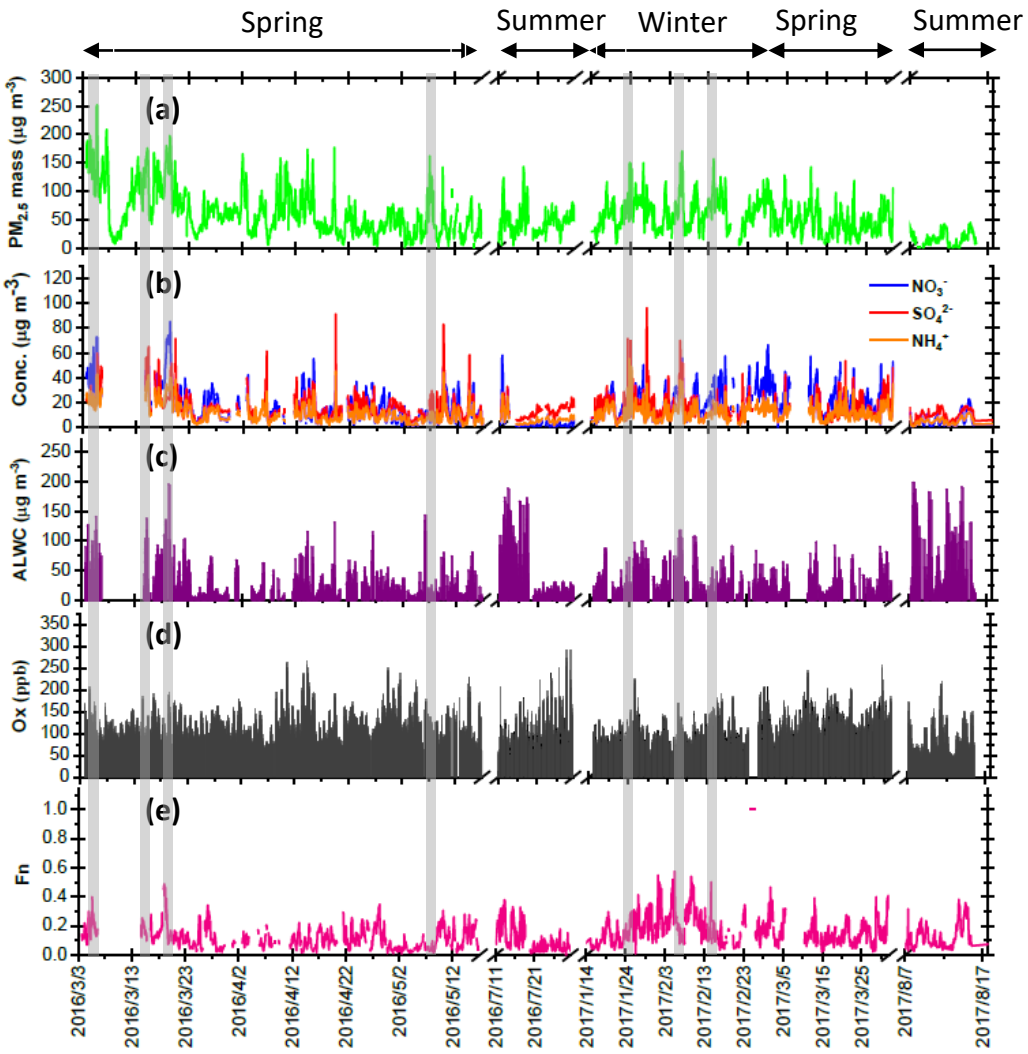

Figure 1 Time series of concentrations in (a) $PM_{2.5}$ mass, (b) SIA species, (c) ALWC and (d) Ox along with (e) Fn observed in Nanjing during the sampling periods. The grey shadows represent the high $PM_{2.5}$ periods discussed in the section 3.6.

(a) Entire days: $PM_{2.5}$ = 58 ± 35 μg m^{-3}

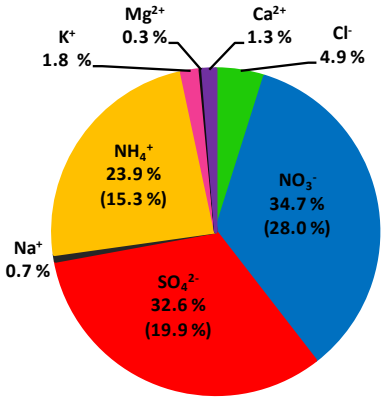

(b) Haze events: $PM_{2.5}$ = 171 ± 18 μg m^{-3}

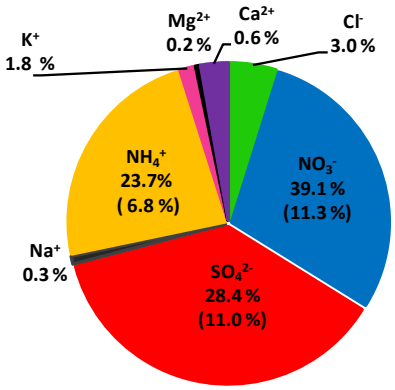

(c) Clear events: $PM_{2.5}$ = 22 ± 9 μg m^{-3}

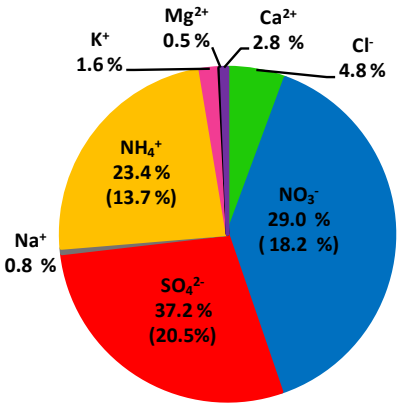

Figurer 2 Abundance of each species in TWSIIs during the (a) entire, (b) haze ($PM_{2.5}$ ≥ 150 μg m^{-3}) and (c) clear ($PM_{2.5}$ < 35 μg m^{-3}) events. The numbers in the parentheses are standard deviations.

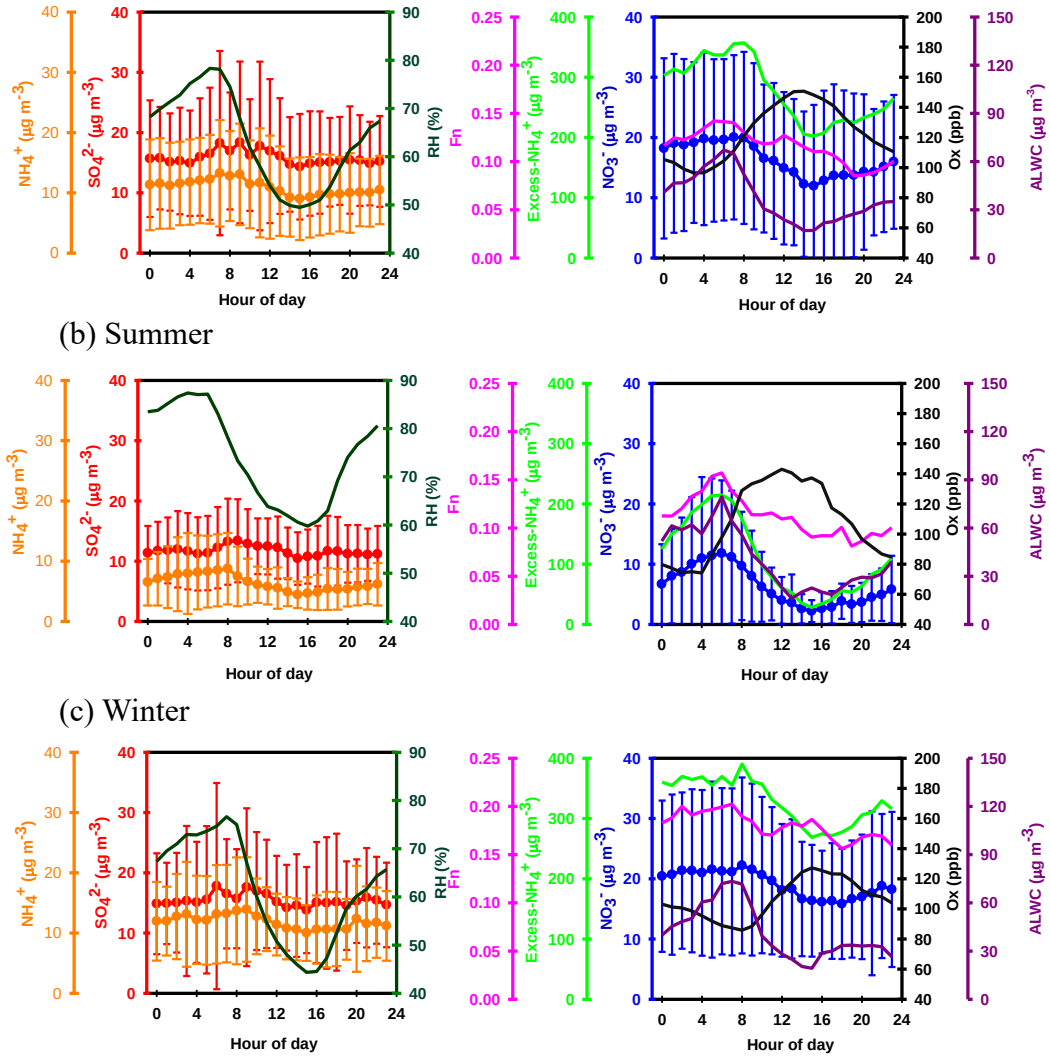

Figure 3 Diurnal variations of the concentrations of NO_3^-, SO_4^{2-} and NH_4^+, excess-NH_4^+, Ox and ALWC, and nitrogen conversion ratio (Fn) as well as ambient relative humidity in Nanjing during the sampling periods. For SO_4^{2-}, NO_3^- and NH_4^+, the mean values (dots) and standard deviations (solid lines) are plotted.

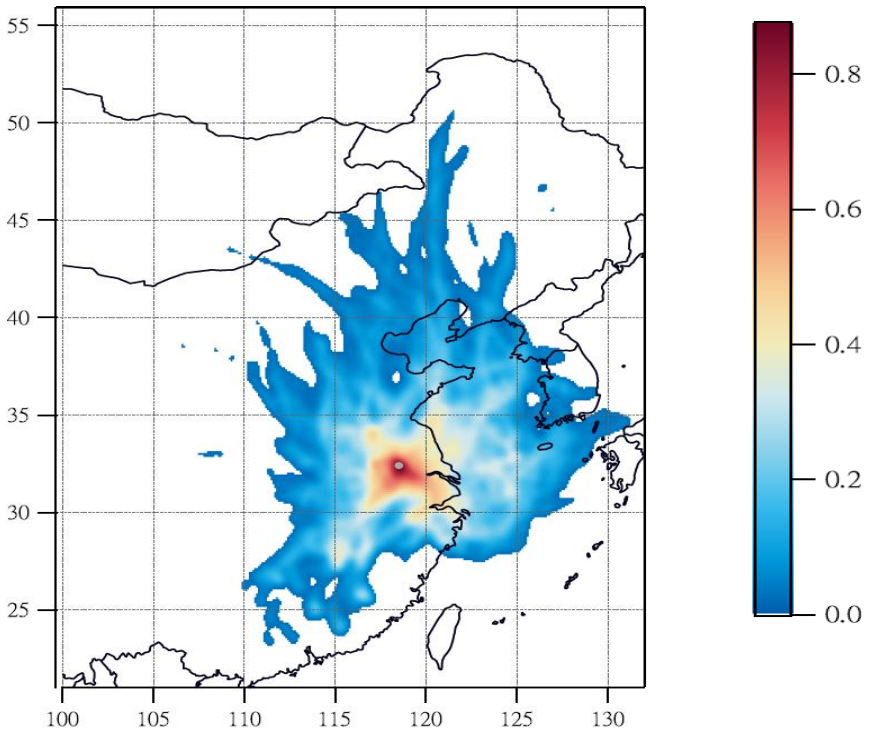

Figure 4 The PSCF maps of high nitrate pollution.

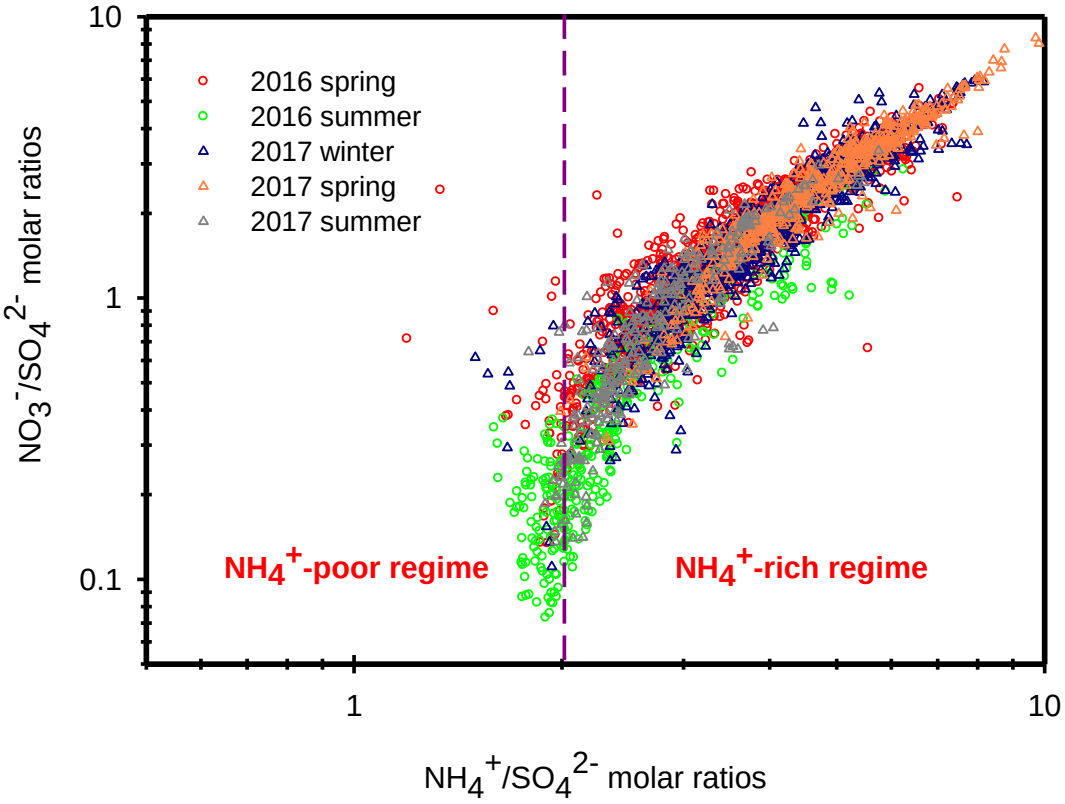

Figure 5 Scatter plots of molar ratios of NO_3^-/SO_4^{2-} against NH_4^+/SO_4^{2-} in Nanjing during the different seasons.

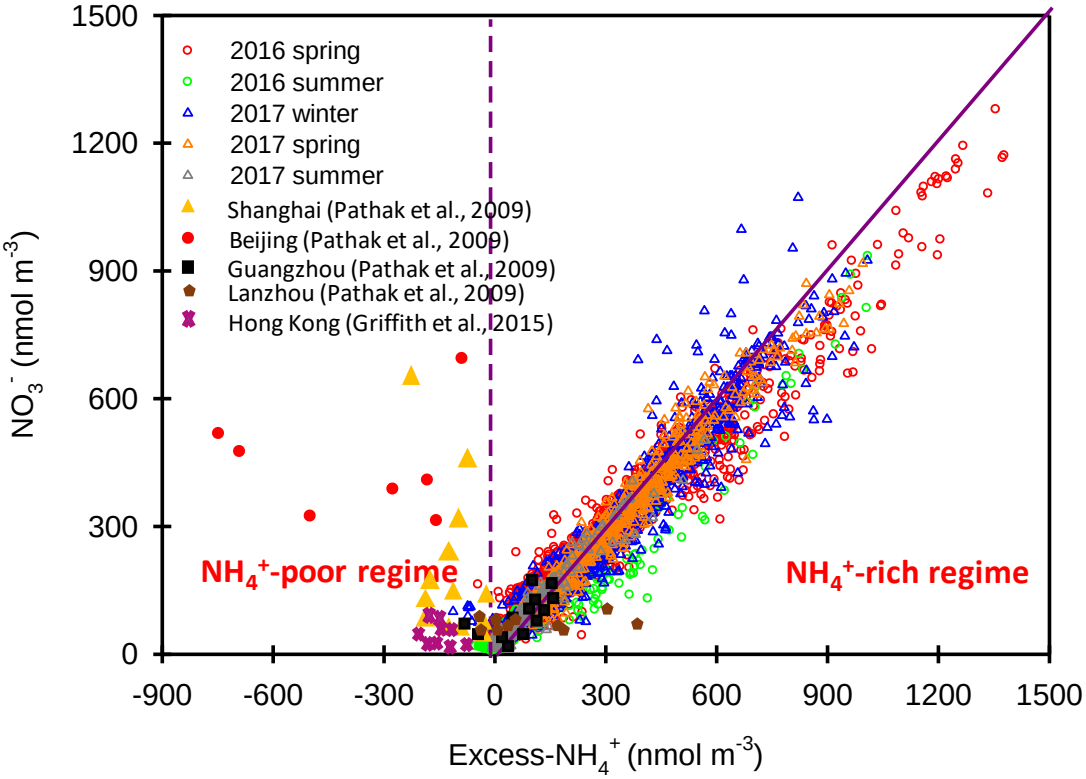

Figure 6 Scatter plot of NO_3^- vs. excess-NH_4^+ molar concentrations in Nanjing during the different seasons. The results in Beijing, Shanghai, Guangzhou, Lanzhou and Hong Kong are also shown in this figure.

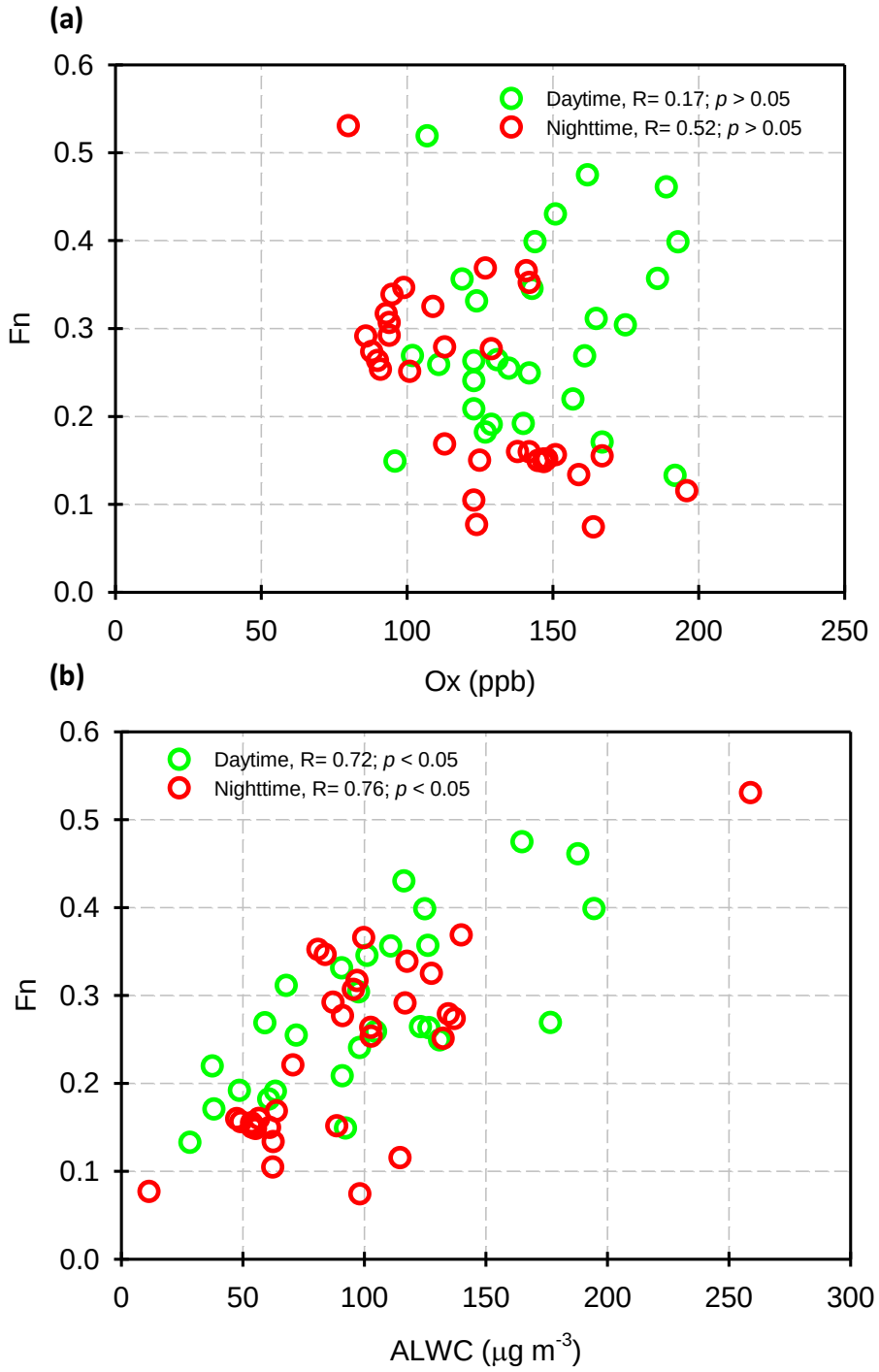

Figure 7 Scatter plots of (a) Fn against Ox and (b) Fn against ALWC in daytime and nighttime aerosol samples during the high hourly $PM_{2.5}$ concentration conditions (hourly $PM_{2.5}$ $\geqq$ 150 μg m^{-3}).

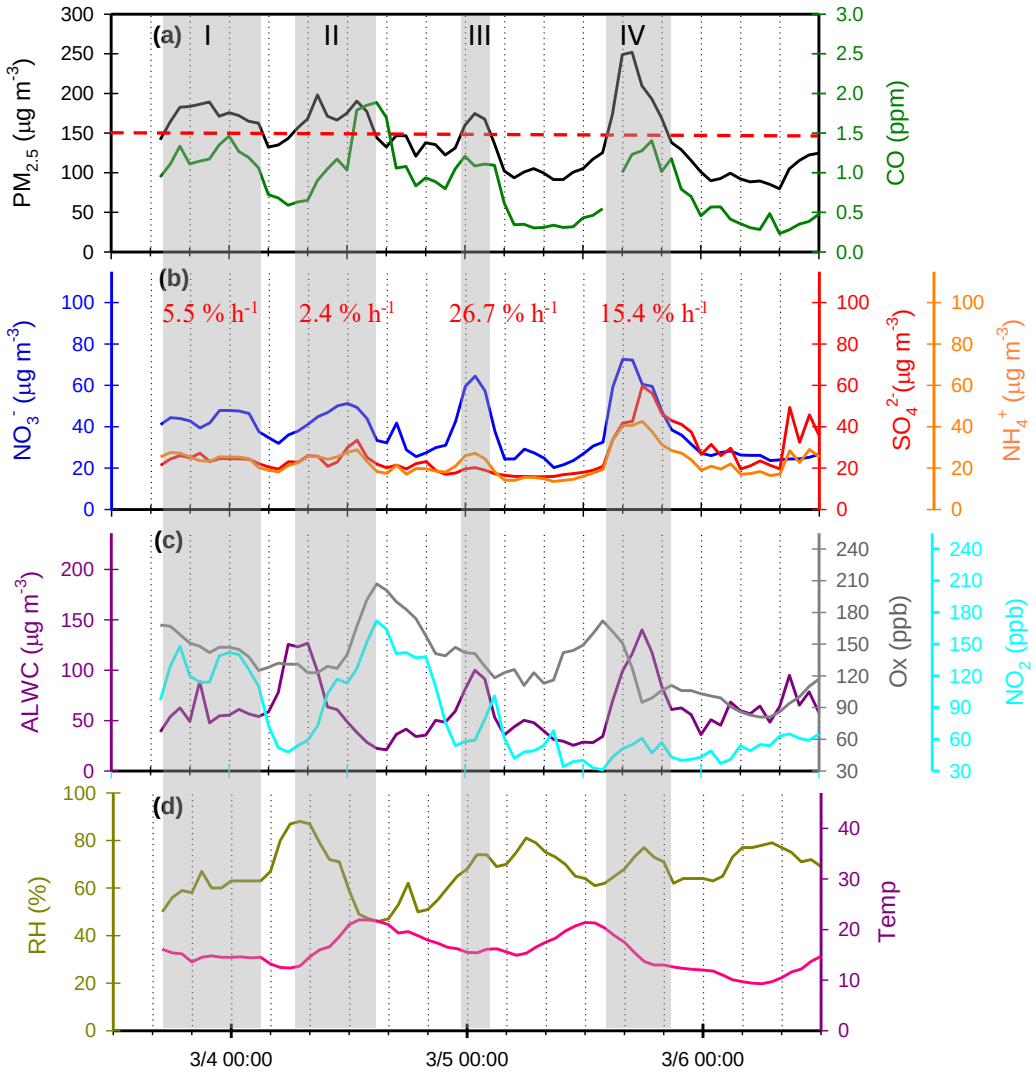

Figure 8 Time series of concentrations in (a) $PM_{2.5}$ mass and CO, (b) SIA species (NO_3^-, SO_4^{2-} and NH_4^+), (c) ALWC, Ox and NO_2 and (d) RH and T in Nanjing City from March 3 to 6, 2016. The grey shadows denote $PM_{2.5}$ episodes. The red numbers represent NO_3^- production rate during the $PM_{2.5}$ episodes.

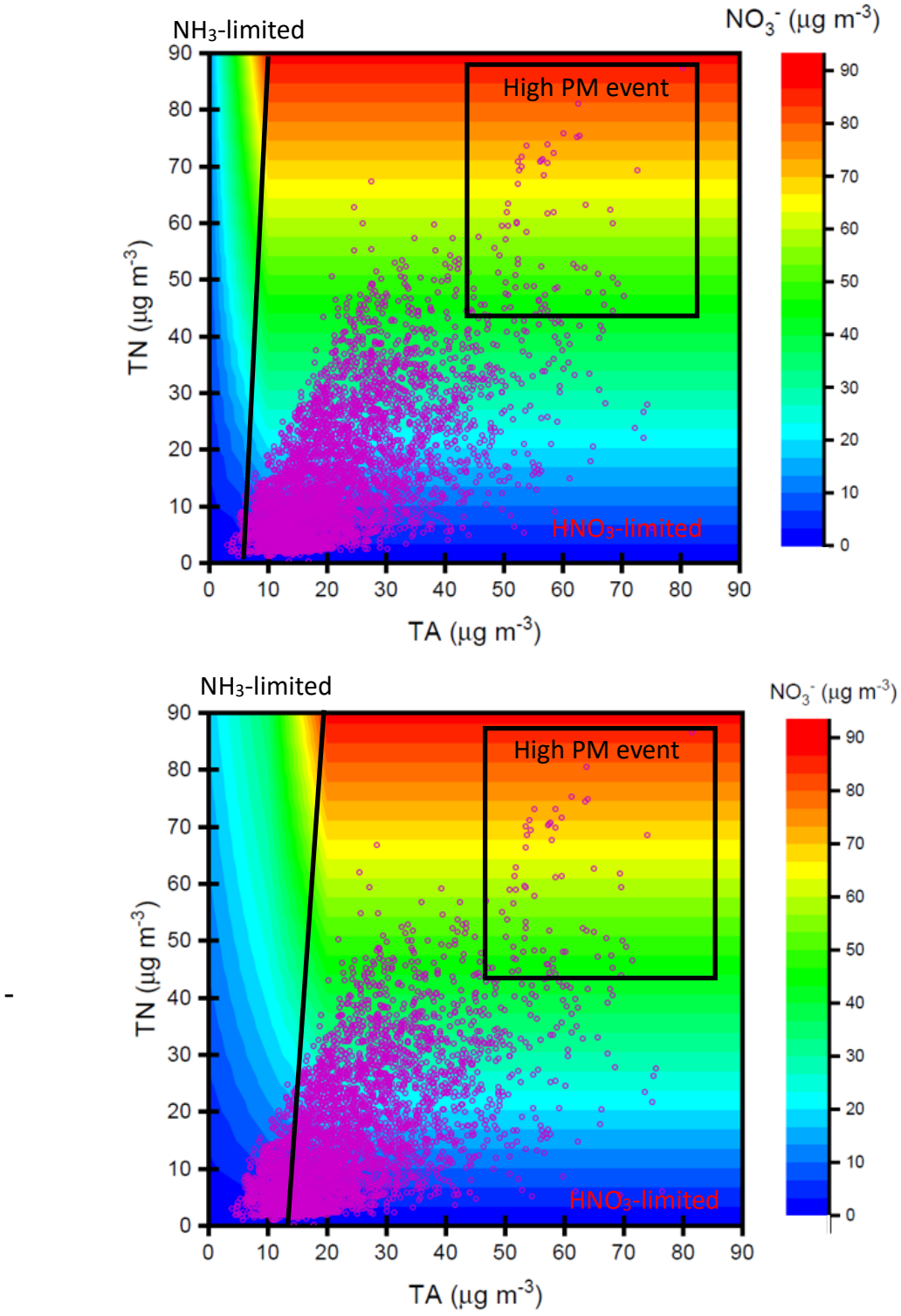

Figure 9 Nitrate concentrations simulated by ISORROPIA II model depending on TN and TA concentrations under (a) SO_4^{2-} = 10 μg m^{-3} and (b) SO_4^{2-} = 60 μg m^{-3}. The purple dots denote the observed TN and TA concentrations at the receptor site during the sampling periods.